Water Research 91 (2016) 235–243

Contents lists available at ScienceDirect

Water Research

journal homepage: www.elsevier.com/locate/watres

Meso and micro-scale response of post carbon removal nitrifying MBBR biofilm across carrier type and loading

Bradley Young [a], Bahman Banihashemi [a], Daina Forrest [a], Kevin Kennedy [a], Alain Stintzi [b], Robert Delatolla [a, *]

[a] Civil Engineering, University of Ottawa, Ottawa, Canada
[b] Ottawa Institute of Systems Biology, Department of Biochemistry, Microbiology, and Immunology, University of Ottawa, Ottawa, Canada

ARTICLE INFO

Article history:
Received 6 September 2015
Received in revised form
4 December 2015
Accepted 5 January 2016
Available online 6 January 2016

Keywords:
Bacterial community structure
Biofilm morphology
Moving bed biofilm reactor (MBBR)
Next generation sequencing
Nitrification

ABSTRACT

This study investigates the effects of three specific moving bed biofilm reactor (MBBR) carrier types and two surface area loading rates on biofilm thickness, morphology and bacterial community structure of post carbon removal nitrifying MBBR systems along with the effects of carrier type and loading on ammonia removal rates and effluent solids settleability. The meso and micro analyses show that the AOB kinetics vary based on loading condition, but irrespective of carrier type. The meso-scale response to increases in loading was shown to be an increase in biofilm thickness with higher surface area carriers being more inclined to develop and maintain thicker biofilms. The pore spaces of these higher surface area to volume carriers also demonstrated the potential to become clogged at higher loading conditions. Although the biofilm thickness increased during higher loading conditions, the relative percentages of both the embedded viable and non-viable cells at high and conventional loading conditions remained stable; indicating that the reduced ammonia removal kinetics observed during carrier clogging events is likely due to the observed reduction in the surface area of the attached biofilm. Microbial community analyses demonstrated that the dominant ammonia oxidizing bacteria for all carriers is *Nitrosomonas* while the dominant nitrite oxidizing bacteria is *Nitrospira*. The research showed that filamentous species were abundant under high loading conditions, which likely resulted in the observed reduction in effluent solids settleability at high loading conditions as opposed to conventional loading conditions. Although the settleability of the effluent solids was correlated to increases in abundances of filamentous organisms in the biofilm, analyzed using next generation sequencing, the ammonia removal rate was not shown to be directly correlated to specific meso or micro-scale characteristics. Instead post carbon removal MBBR ammonia removal kinetics were shown to be related to the viable AOB cell coverage of the carriers; which was calculated by normalizing the surface area removal rate by the biofilm thickness, the bacterial percent abundance of ammonia oxidizing bacteria and the percentage of viable cells.

1. Introduction

The moving bed biofilm reactor (MBBR) was initially developed as a nitrogen removal system in the 1980's (Rusten et al., 1994) and quickly evolved to operate effectively as a chemical oxygen demand (COD) removal system (Ødegaard et al., 1994). The MBBR system houses biocarriers with attached biofilm, and as such the removal of the carbonaceous and nitrogenous constituents occurs through mass transfer into the biofilm and the subsequent metabolic processing of these constituents by bacterial cells. Thus, the performance of MBBR systems, measured at the macro-scale of influent and effluent concentrations, is ultimately dependent upon the meso-scale properties of the biofilm and the micro-scale bacterial cell community.

It is well known that diffusion into biofilm is dependent on flow velocities across the biofilm with increases in flow velocity resulting in larger localized concentration gradients in the biofilm and faster rates of diffusion through the biofilm. Flow velocity changes can result from carrier orientation, carrier pore space configuration and the geometry of the biofilm surface (Herrling et al., 2014; Li et al., in press). Thus the applied loading and MBBR carrier type

* Corresponding author. Department of Civil Engineering, University of Ottawa, 161 Louis Pasteur, K1N 6N5 Ottawa, ON, Canada.
E-mail address: robert.delatolla@uottawa.ca (R. Delatolla).

http://dx.doi.org/10.1016/j.watres.2016.01.006
0043-1354/

used could influence the morphology and thickness of the biofilm matrix and subsequently affect the rate of mass transfer of nutrients and substrates to the microbial community embedded in the biofilm.

Previous work on COD removal MBBR systems have concluded that system performance is not dependent on carrier type but instead is a function of surface area loading rate (Ødegaard et al., 2000). In this work however, Ødegaard et al. (2000) found inexplicable differences in effluent biomass settleability from the two different carrier types used in their study; indicating the possibility of a difference in biofilm morphology between different carriers and highlighting a potential variability in the bacterial communities. Martín-Pascual et al. (2012) has more recently shown that three MBBR systems with different carriers operated at various hydraulic retention times (HRTs) and filling ratios showed different COD removal efficiencies. Furthermore, additional studies have also shown increases in biofilm thickness as a response to increases in loading rates, which can be achieved through variations in HRT and fill fractions (Wang et al., 2005; Karizmeh et al., 2014). COD removal MBBR systems were shown to exhibit distinct morphologies at various loading conditions, with low density porous structures observed at low loading and filamentous-like morphologies observed at higher loading (Karizmeh et al., 2014). These distinct morphologies suggest a potential difference in the microbial communities within the biofilm.

To date there are limited studies examining the effects of carrier type and loading rate on nitrifying and nitrogen removal MBBR systems. In particular, no research exists in the literature on biofilm thickness, morphology and microbial population community shifts in response to carrier types and surface area loading rates in nitrifying MBBR systems. Population shifts have been observed in nitrifying trickling filters, with low ammonia environments being dominated by *Nitrosospira*, while high ammonia concentrations were shown to harbour *Nitrosomonas* as the dominant AOB (Zhang et al., 2013). The study also found *Nitrobacter* to be the dominant NOB with high substrate availability and *Nitrospira* being dominant during starved conditions.

Nitrifying MBBR treatment basins are conventionally located downstream and separate from carbon removal MBBR basins in municipal wastewater treatment trains to minimize the adverse effects of carbon removing heterotrophic populations overgrowing and smothering the nitrifying autotrophic populations (Nogueira et al., 2002; Lee et al., 2004). Further, nitrifying MBBR systems have become increasingly popular as lagoon upgrade systems with the implementation of more stringent ammonia discharge regulation (WEF, 2011; Canada Gazette, 2012). These systems perform as cost effective, efficient, post carbon removal upgrade systems to current passive lagoon treatment systems that do not achieve ammonia removal. A true understanding of the meso and micro-scale effects of carrier type and loading on post carbon removal nitrifying MBBR systems is critical to further develop and optimize these cost-effective treatment systems. Therefore the aim of this study is to establish the effect of carrier type and ammonia loading rate at the meso and micro-scale within post carbon removal nitrifying MBBRs. In particular, this study focuses on biofilm thickness and morphology, cell viability and bacterial community analysis in response to carrier type and variations in ammonia loading as well as their correlation to ammonia removal rates and effluent settleability.

2. Material and methods

2.1. Reactor configurations and synthetic wastewater

Four lab scale reactors with three different carrier types were operated under identical conditions at two distinct loading conditions, a high loading condition (HLC) of a surface area loading rate (SALR) of 1.89 g-N/m^2 d and a conventional or normal loading condition (NLC) of an SALR of 0.9 g-N/m^2 d. The total operation time of the four reactors (including start-up, HLC, transition phase to NLC, and NLC) was approximately 2160 HRT cycles (9 months) In particular, the start-up phase was approximately 1200 HRT cycles (5 months); the steady state HLC phase occurred over a periods of 300 HRT cycles (approximately 38 days); the transition phase to NLC conditions occurred over a period of 225 HRT cycles (approximately 28 days); and the steady state NLC phase occurred over a period of 435 HRT cycles (approximately 54 days) where steady state was defined as less than 10% variation in nitrification kinetics and effluent concentration. The reactors were operated at a conventional HRT of 3 h (WEF, 2011), pH of 8.0 ± 0.1, a dissolved oxygen concentration (DO) of 9.0 ± 0.9 mg/l and were fed with synthetic wastewater. A synthetic wastewater was used throughout the experimental phase to provide stable loading rates with limited variations. Synthetic wastewater (modified version of Delatolla et al., 2009) with an influent ammonia concentration of 50 mg-N/L was used to feed the reactors throughout the HLC experimental phase to provide stable loading rates with limited variations: $(NH_4)_2SO_4$: 235.82 mg/L, $NaHCO_3$: 650 mg/L, $MgSO_4.7H_2O$: 325 mg/L, $CaCl_2.2H_2O$: 29.34 mg/L, KH_2PO_4: 79.09 mg/L, $FeSO_4.7H_2O$: 4.98 mg/L. Carbon source: $C_6H_{12}O_6$: 3.8 mg/L, NaAc: 2.0 mg/L, Peptone: 3.8 mg/L. Trace nutrients included $MnCl_2.4H_2O$: 200 μg/L, $NaMoO_4.2H_2O$: 49.62 μg/L, $CuSO_4.5H_2O$: 205.1 μg/L, $CoCl_2.6H_2O$: 2 μg/L, $ZnSO_4.7H_2O$: 59.82 μg/L.

The glucose, acetate and peptone were supplied to mimic the readily degradable carbonaceous content of wastewater at a concentration of 10 mg BOD_5/L under HLC. Nitrifying MBBR systems are conventionally designed, with respect to BOD_5 concentration, to achieve $BOD_5 < TKN$ and $sBOD_5 < 12$ mg/L in order to minimize the adverse effects of heterotrophic overgrowth on autotrophic nitrifiers in the same treatment basin (WEF, 2011). Hence, nitrifying MBBR basins are conventionally designed separate to carbon removal MBBR units, with nitrifying MBBR basins being located downstream of carbon removal MBBR units or carbon removal lagoon treatment units. Nitrification is often inhibited year round in northern country lagoon treatment systems due to the effect of winter operation and furthermore the ammonia concentrations have been shown to increase in the lagoon due to the process of ammonification that occurs in the settled sludge bed in the lagoons. The NLC concentrations and loadings of the carbonaceous and nitrogenous substances to the nitrifying MBBR reactors in this study was based on conventional municipal treatment systems in multi-basin MBBR treatment systems and post lagoon treatment conditions that does not achieve ammonification. The HLC concentrations and loadings of the carbonaceous and nitrogenous substances were based on post carbon removal lagoon treatment where ammonification occurs in the settled sludge bed of the lagoon and has increased the ammonia concentration in the lagoon effluent.

After the reactors were analyzed at steady state HLC, the ammonia, alkalinity and BOD_5 were gradually decreased to proportionally half of the concentrations at HLC to maintain the same nitrogen to alkalinity and nitrogen to carbon ratios at NLC operation.

Reactors 1 and 2 were 2 L cylindrical reactors operating with 50% fill of K3 AnoxKaldnes biofilm carriers. The K3 carrier is 25 mm in diameter and 12 mm in depth with an available surface area of 500 m^2/m^3 (WEF, 2011). Reactors 3 and 4 were 1.2 L cylindrical reactors operating with 30% fill of the AnoxKaldnes P carrier and 20% of the AnoxKaldnes M carrier, respectively. The P carrier is 2 mm in depth with a diameter of 48 mm and available surface area

of 900 m^2/m^3, while the M carrier is 2 mm in depth with a diameter of 48 mm and a surface area for biofilm attachment of 1200 m^2/m^3 (WEF, 2011). Reactors 3 and 4 were sized differently from reactors 1 and 2 to promote better rotation of the P and M carriers in the reactors. Specifically, the modified diameter to height ratio of reactors 3 and 4 enabled better rotation of the P and M carriers, while potentially minimizing the wall effects on the carriers (Leyva-Díaz et al., 2013). The air inflow rate of the reactors containing the K3, M and P carriers was approximately 4, 3, and 3 L/min, respectively. The rate of aeration in each reactor was designed to maintain constant rotation of the carriers in the reactors while supplying sufficient oxygen for the necessary biological processes. Based on the aeration requirement for carrier movement in the reactors, the DO concentrations were maintained at 9.0 ± 0.9 mg/l throughout the entire study. As the effluent ammonia concentrations and hence the reactor bulk phase ammonia concentrations were below 5 mg-N/L throughout the study, the kinetics of the reactors were likely ammonia mass transfer rate limited and not oxygen mass transfer rate limited (WEF, 2011); hence minimizing the effects of elevated DO concentrations on the kinetics of the study.

2.2. Constituent analysis

Effluent concentrations of ammonia, nitrite and nitrate were measured in accordance with standard methods (APHA et al., 1998); methods 4500- NH_3, 4500-NO_3^- B, and 4500-NO_2^-. DO and pH measurements were acquired using a symphony Multi Parameter Meter with attached DO and pH probes (VWR, Canada, Ontario). Temperature within the reactors was measured daily using a mercury glass thermometer and maintained at 22 ± 1 °C by the thermostat controlled environment within the laboratory. Total suspended solids (TSS) and volatile suspended solids (VSS) were measured according to Standard Methods (APHA et al., 1998); 2540 D- Total Suspended Solids (total suspended solids dried at 103–105 °C), 2540 E– Volatile Suspended Solids (volatile solids ignited at 550 °C). All wastewater constituent samples were collected in triplicate and were filtered through a 0.45 μm filter before testing to reduce the effect of suspended solids on measured values.

2.3. Settleability of effluent solids

Due to the fact that the nitrifying MBBR process produced a low concentration of effluent TSS, the sludge volume index (SVI) of the samples could not be measured accurately for this study. Hence, the settleability of the solids produced by the reactors was investigated using a digital particle analyzer (Brightwell Technologies Inc., Canada, Ontario). Digital particle analysis (DPA) enabled the distribution of particles between 2.25 μm and 400 μm to be measured. Using DPA to quantify the particle distribution of the solids prior to and following 30 min of settling enabled the settleability of the solids to be quantified in this study. Five effluent samples were collected from each reactor and the DPA measurements of each sample was analysed in triplicate.

2.4. Microbial analysis

2.4.1. Biofilm morphology and mass

Biofilm morphology and thickness were observed through the use of a Vega II-XMU variable pressure scanning electron microscope (VPSEM) (Tescan USA Inc., USA, Pennsylvania). During each phase of the study a carrier was randomly selected from each reactor and without sample preparation analysed in the VPSEM chamber at 40 Pa. The VPSEM was optimized to 40 Pa pressure for maximum exposure of 5 min to prevent morphological changes due to dehydration. Images were acquired at 20 points across the carrier with magnifications ranging from × 20 to × 5000. Though VPSEM may produce shrinkage of the biofilm with long exposure (exposures times were restricted in this study to minimize biofilm shrinkage), it eliminates the need for destructive sample preparation which is a necessity of traditional SEM (Flemming et al., 2000; Delatolla et al., 2009b).

Three carriers were harvested from the reactors to measure the mass of biofilm on the carriers. The carriers were centrifuged in 85 mL centrifuge tubes for 30 min at 9000 rpm in a Sorvall centrifuge (Thermo Fisher Scientific, Massachusetts, USA). Subsequently, the samples were vortexed using a vortex-genie (Fisher Scientific, New York, USA) for 15 min at a maximum speed of 10. The TS and VS were measured on the resultant extracted biofilm according to Standard Methods (APHA et al., 1998): 2540 B – TS and 2540 E – VS.

2.4.2. Cell viability

One carrier was randomly selected from each reactor for analysis during both HLC and NLC. The carrier was cut to expose the inner surfaces and stained with Propium Iodide and Syto 9 of the film Tracer™ LIVE/DEAD® biofilm viability kit (Life Technologies, Ontario, Canada) along with calcofluor to illuminate the extracellular polymeric material of the biofilm in blue. Confocal light scanning microscopy (CLSM) has become a conventional method for the enumeration of micro-organisms on surfaces and the characterization of biofilms. CLSM allows for the non-destructive optical sectioning of the biofilm. An LSM 510/Axio imager M.1 confocal microscope (Carl Zeiss Canada Ltd, Ontario, Canada) equipped with argon and helium-neon lasers was used to image the biofilm samples in this study. A total of 20 images per reactor or 4 stacks of 5 images acquired within an approximate total depth of 30 μm were captured for each sample and were analysed using NI Vision Assistant 7.1 (LabView 8.0- National Instruments Canada, Vaudreuil-Dorion, Canada). The biofilm area and the area of the fluorescent red and green illuminated cells were quantified (Delatolla et al., 2009b).

2.4.3. DNA extraction and amplification

For each set of microbial community data five replicate carriers randomly selected from each reactor. For each carrier, 0.25 g of biofilm was abraded from the media into a 1.5 mL sterilized Eppendorf tube. DNA was extracted from the biofilm using FastDNA® spin kit (MP Biomedicals, Santa Ana, CA) and the DNA was stored at −80 °C until it was used for library construction. DNA amplification utilized a two-step polymerase chain reaction (PCR) targeting the V6 hyper-variable region of the 16s rRNA was achieved using Phusion® High-Fidelity PCR Master Mix (Thermo Fisher Scientific Inc., Waltham, MA). The primers used for the first and second PCR reaction were selected from a barcoding approach previously described by Abujamel et al. (2013). The PCR amplicons were inspected by electrophoresis on a 2% agarose gel and purified with a Montage PCR96 cleanup kit (EMD Milipore, Billerica, MA). The purified amplicons were quantified using Quant-iT™ dsDNA HS Assay Kit (Life Technologies, Burlington, Canada) and pooled with 200 ng of DNA from each sample to be sequenced using an Illumina Hiseq2500 at the center for applied genomics (TCAG, Toronto, Canada).

2.4.4. DNA sequencing analysis

The entire DNA sequencing analysis was disseminated using Bio Linux operating platform. The paired-end reads were assembled using the fast length adjustment of short reads (FLASH) software (Majoc and Salzberg, 2011) and quality filtered using the Fastq_quality_filter command from the Fastx toolkit with the minimum

quality score of 20 over 97% of the sequences. Reads that passed the quality filter were demultiplexed and the barcodes were trimmed using Novobarcode (Goecks et al., 2010). The quantitative insights into microbial ecology (QIIME) software, version 1.8, (Majoc and Salzberg, 2011) was used to compute operational taxonomical unit (OTU) clustering with a closed reference of 97% sequence similarity. QIIME compared the OTUs with UCLUST against the Greengenes database 13.8; the singletons were removed and the relative abundance of the bacterial taxa present in the biofilm was determined (Caporaso et al., 2010). The biofilm samples were highly diverse with greater than 800 species per sample. To ensure adequate coverage for subsequent analysis and minimize false positives due to low read numbers, samples with less than 15,000 species per sample were removed from the sample set (with a total of 5 samples being analyzed for each carrier at HLC and NLC). The samples with greater than 15,000 reads were analyzed for differential abundance of bacterial taxa using metagenomeSEQ (Paulson et al., 2013).

2.5. Microbial activity

In this study kinetic rates were normalized with respect to the biofilm thickness, cell viability, and AOB relative abundance. The ammonia removal rate was expressed per biofilm volume by dividing the SARR by the biofilm thickness in an aim to evaluate the biofilm volume ammonia removal rate (BVRR) across carrier type and loading conditions (Hoang et al., 2014)

$$\mathrm{BVRR} = \frac{\mathrm{SARR}}{B_T} \tag{1}$$

Where BVRR is biofilm volume ammonia removal rate (g-N/m^3 d), SARR is surface area removal rate (g-N/m^2 d) and B_T is biofilm thickness (m).

The ammonia removal rate was also expressed per viable cell volume by dividing the SARR by the viable cell coverage of the biofilm in order to evaluate the viable cell ammonia removal rate (VCRR) across carrier type and loading conditions (Hoang et al., 2014). Previous work has shown a rapid decrease in oxygen and substrates from the surface of the biofilm to the carrier support, which could a decrease in cellular kinetics (Li et al., in press). To account for potential loss in cellular kinetics, the viable cell coverage of the biofilm was interpolated through the entire measured biofilm thickness based on the CLSM viable cell data analysed for the upper 30 μm thick biofilm section of the samples. Interpolation used a least squares fitting method to interpolate the live cell coverage for the entire thickness of the biofilm for each carrier.

$$\mathrm{VCRR} = \frac{\mathrm{SARR}}{B_T \times L_C} \tag{2}$$

Where VCRR is viable cell ammonia removal rate (g-N/m^3 d) and L_C is percent live cell coverage (%).

Furthermore, the ammonia removal rate is also expressed per viable AOB cell volume by dividing the SARR by the viable AOB cell coverage (VAOBRR) across carrier type and loading conditions. This analysis uses the interpolated viable cell coverage above and assumes the viable cell coverage is uniform across the bacterial population.

$$\mathrm{VAOBRR} = \frac{\mathrm{SARR}}{B_T \times L_C \times \%AOB} \tag{3}$$

Where VAOBRR is viable AOB ammonia removal rate (g-N/m^3 d) and %AOB is the relative abundance of AOB.

2.6. Statistical analysis

All constituent statistical analyses were based on 5 samples taken in triplicate (15 measurements); biofilm thicknesses were based on 20 measurements acquired from 5 images; cell viability analyses were based on 20 acquired images and sequencing percent abundances were based on 5 replicate samples. Statistical significance of measured constituents, biofilm thickness, cell viability and percent abundance values across carrier types and between the two loading phases were tested by the t-test with a p-value of 0.05 for statistical significance using GraphPad Prism 6. All constituent, biofilm thickness, cell viability and percent abundance samples were acquired at steady state.

For the bacterial community shift analysis, statistical significance within the weighted uni-frac beta diversity was tested using nonparametric statistical method (ADONIS) from the program QIIME (Caporaso et al., 2010). Statistical significance within the taxa was tested using a zero inflated Gaussian model incorporated into the metagenomeSEQ package.

3. Results and discussion

3.1. Nitrifying kinetics

High removal efficiencies of ammonia were observed at both HLC and NLC with average system removal efficiencies of 93.6 ± 3.0% at HLC and 97.6 ± 1.0% at NLC and with surface area removal rate (SARR) values of 1.82 ± 0.01 and 0.89 ± 0.01 g-N/m^2·d, respectively (Fig. S1). The effluent ammonia concentrations of all reactors were below 2 mg-N/L, with the exception of the M carrier at HLC that was 4.70 ± 2.45 mg-N/L (Table S1). All reactors showed limited nitrite accumulation, with effluent nitrite concentrations remaining less than 1 mg-N/L in all reactors at HLC and NLC (Table S1). No significant difference in substrate removal rates was observed for different carrier types at HLC or NLC with the exception of the M carrier at HLC (Fig. S1a). Other studies also showed more stability in ammonia removal rates for K3 carriers at various loading conditions (Zhang et al., 2013; Gilbert et al., 2015). The lower SARR values of the M carrier compared to other carriers at HLC is attributed to the clogging of the carrier's pore spaces due to excessive biofilm growth; leading to reduced biofilm surface area for substrate penetration. The clogging of the M carriers not only showed lower SARR values but also demonstrated small fluctuations in the effluent ammonia concentrations as compared to the other carriers that remained unclogged at higher loading. Hence, the type of carrier used in MBBR systems showed little effect on nitrifying kinetics for all unclogged carrier conditions. However, at high loading condition the highest surface area to volume ratio carrier showed a tendency to clog and subsequently lower its removal efficiency and the stability of the effluent ammonia concentrations.

3.2. Settleability of effluent solids

The average percentage of effluent particles removed by 30 min of settling at HLC for all carriers was 45 ± 19%. The result of effluent particles removal for each carrier shows that the P carrier (59 ± 21%) and the K3 carrier (56 ± 25%) produce effluent with significantly better settling characteristics than the M carrier (11 ± 5%). The effluent of the M carrier reactor at HLC showed the poorest solids settlement, which coincides to a clogging of the carriers and the subsequent slower kinetics compared to the other carriers.

At NLC the average percent settlement of effluent particles was 70 ± 6%, the M and P carrier demonstrated similar settling (79 ± 3%

and 79 ± 4%) and the K3 carrier (62 ± 9%) showed the least settlement. Hence, the study shows that higher nitrogen loading conditions cause a reduction in particle settleability. This is in agreement with previous studies on carbon loaded MBBR systems that showed poor biomass settleability at higher carbon loads (Ivanovic et al., 2006; Ivanovic and Leiknes, 2012).

3.3. Biofilm morphology and mass

The morphology and mass results (Fig. 1) show thicker biofilms with greater biofilm mass per reactor at HLC than NLC. This observation is expected as higher loadings promote deeper substrate penetration into the biofilm as well as a thicker biofilm (Gerardi, 2002). The morphology and mass results also offer a comparison of the biofilm growth across different carrier types and demonstrate no significant differences in biofilm thickness or biofilm mass per reactor between the K3 and P carriers at HLC. However the biofilm thickness of the M carrier (carrier with the highest surface area to volume ratio) at HLC differs significantly compared to both the K3 and P carriers. The significantly thicker biofilm of the M carrier at HLC corresponds to the clogging of the M carrier. Under HLC the clogged M carrier demonstrated significantly higher biofilm mass per reactor measurements compared to K3, significantly lower SARR values and lower effluent solids settleability compared to the K3 and P carriers in addition to demonstrating small fluctuations in the effluent ammonia concentrations. These fluctuations were likely a result of limitation of substrate penetration into the biofilm. For example, it has been shown on average the maximum penetration depth of oxygen in an aerobic reactor is 100–150 μm (Tijhuis et al., 1994). The depth of penetration in this study was likely to be at the higher boundary due to oxygen saturation in the bulk liquid, however, the clogged M carrier significantly exceeded the maximum penetration depth of oxygen. This would have created anoxic zones at depth in the biofilm and likely caused the operational instability.

Under NLC the M and P carriers (carriers with higher surface to volume ratios compared to the K3 carriers) show a significantly greater biofilm thickness than the K3 carrier where M had the highest biofilm thickness, with the biofilm mass per reactor not demonstrating a significant change across carriers; during this phase however the SARR value of the M and P carriers was similar to the SARR of the K3 carrier. Therefore for nitrifying MBBRs biofilm thickness and biofilm mass per reactor are not direct indicators of system performance; however under high loading conditions excessive growth promotes clogging which can significantly reduce the nitrifying kinetics. Furthermore, the biofilm thickness, biofilm mass per carrier and the solids settlement results for the studied carriers at NLC, suggest that excessive biofilm growth produces solids with a greater propensity to settle within 30 min.

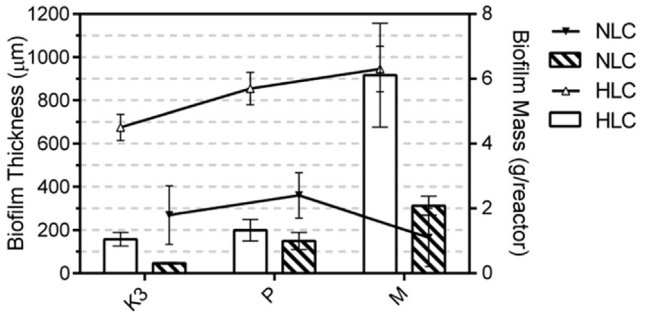

Fig. 1. Average and 95% confidence interval values of measured biofilm thickness and biofilm mass per reactor across carrier type and loading condition (data sets acquired after three weeks of steady state operation).

Researchers studying MBBR carbon loaded systems were able to observe distinct differences in the biofilm morphology between different loading conditions; clear shifts from thick to fibrous films and clear changes in density (Karizmeh et al., 2014). Fibrous structural elements were not observed in the nitrifying biofilm grown of this study (Fig. 2). The acquired VPSEM images do however highlight differences in the protozoa, nematodes and water mite communities across carrier type and across loading conditions. At HLC an abundance of water mites on the K3 carrier is observed (Fig. 2a), as well as their lack of absence on the P and M carriers (Fig. 2b and c). In addition there are numerous ciliates present at the surface of the P and M carriers biofilm at HLC, which are absent from the K3 carrier. Stalked ciliates were seen to be the predominant feature on the P carrier (Fig. 2b) while free-ciliates and nematodes tend to be more dominant on the M carrier (Fig. 2c). These results demonstrate that the meso-scale environments developed on each carrier type differ and that the micro-scale results may also differ; as a result each carrier type may promote the proliferation of different abundances of microorganisms. At NLC the VPSEM images of all carriers show the absence of the protozoa, nematodes and water mites observed at HLC and at NLC distinctly thinner biofilms are observed as compared to HLC. Further, Fig. 2c demonstrates that the clogging of the M carriers was not uniform across the pore spaces. It is evident that not all pore spaces are completely clogged by biofilm, but some pores spaces maintained their integrity and others were partially clogged which indicates that the effective surface area of the biofilm attached to the M carrier at HLC is reduced as excess biofilm grows in the carriers pore spaces (Fig. 2c).

3.4. Cell viability

The viability test illuminates viable cells in green and non-viable cells in red and was used in this study in combination with confocal microscopy to capture images of cell viability at five distinct depths in the biofilm of the harvested samples (Fig. S2). The percent of viable and non-viable cells were quantified in the upper 30 μm thick biofilm section of the samples (Fig. 3). Viability analysis was limited to a depth of 30 μm to ensure that when analyzing carrier samples with thinner biofilm (with an approximate minimum thickness of 30 μm) the same depths and number of images acquired for each sample analyzed was consistent throughout the study. Further, the upper 30 μm of the biofilm is believed to be the most active section of the biofilm.

No significant difference was observed between HLC and NLC with respect to the percent of viable cells, percent of non-viable cells or percent of total cells per area of biofilm for each of the carriers (Fig. 3). No difference in percentage of total cells was observed at HLC as compared to NLC despite the fact that significantly thicker biofilms were shown at HLC as compared to NLC.

The research was also aimed at determining effects of carrier type on the viability of the biomass. The various carriers investigated in this study demonstrated similar percent coverage of viable cells per biofilm area irrespective of carrier type at HLC and NLC (Fig. 3). The M and P carriers, however, did demonstrate a significantly lower percent coverage of non-viable cells as compared to K3 carriers at NLC. This significant difference in non-viable cell coverage can be due to the fact that the M carriers were consistently clogged during operation at HLC. Subsequently, during the transition from HLC to NLC a large change in biofilm thickness occurred in the M carrier, where the thickness of the biofilm was reduced by approximately one-third (Fig. 1). This sloughing of the biofilm thickness may have exposed deeper areas of biofilm that was less active due to restrictive mass transferring of nutrients and

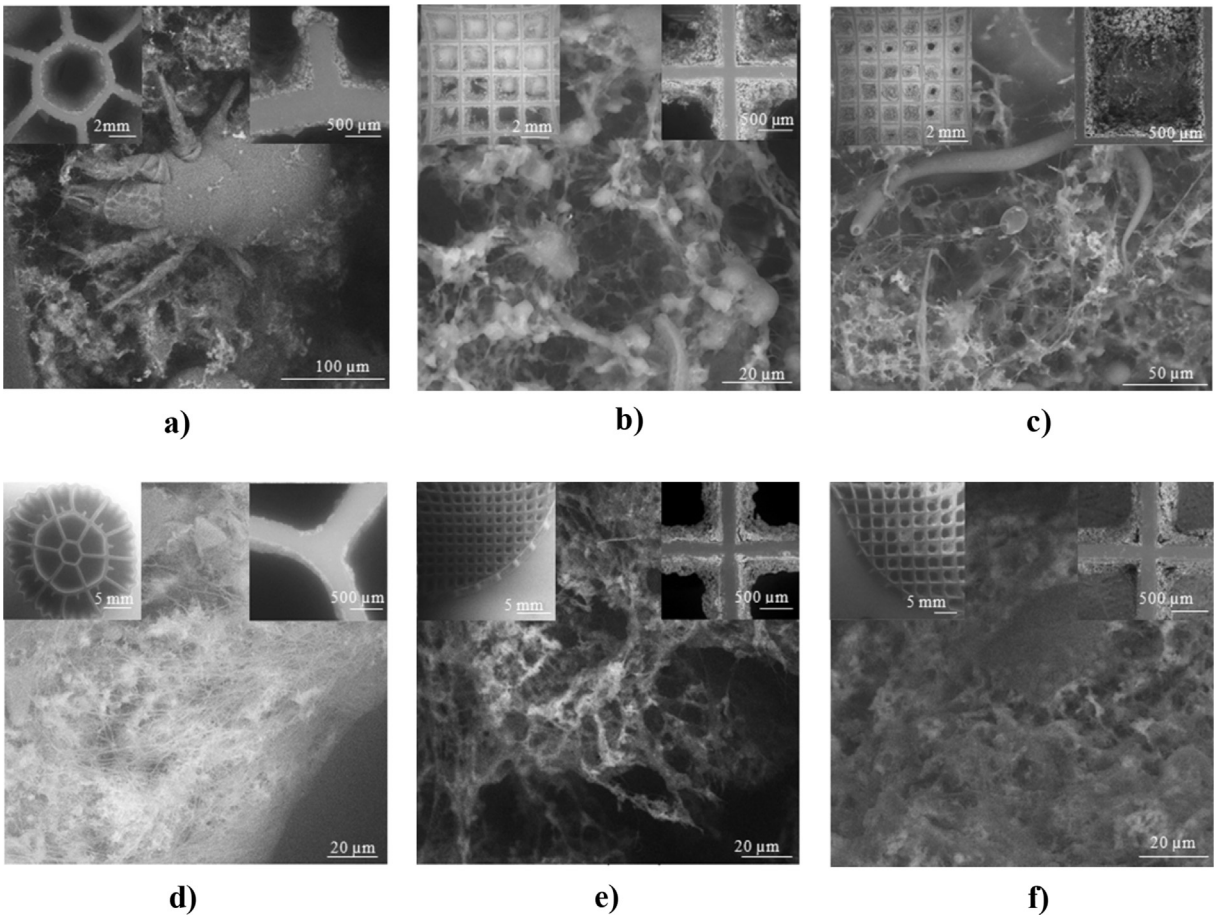

Fig. 2. VPSEM images acquired after three weeks of steady state operation; a) K3 carrier-HLC, b) P carrier-HLC, c) M carrier-HLC, d) K3 carrier-NLC, e) P carrier-NLC, f) M carrier-NLC.

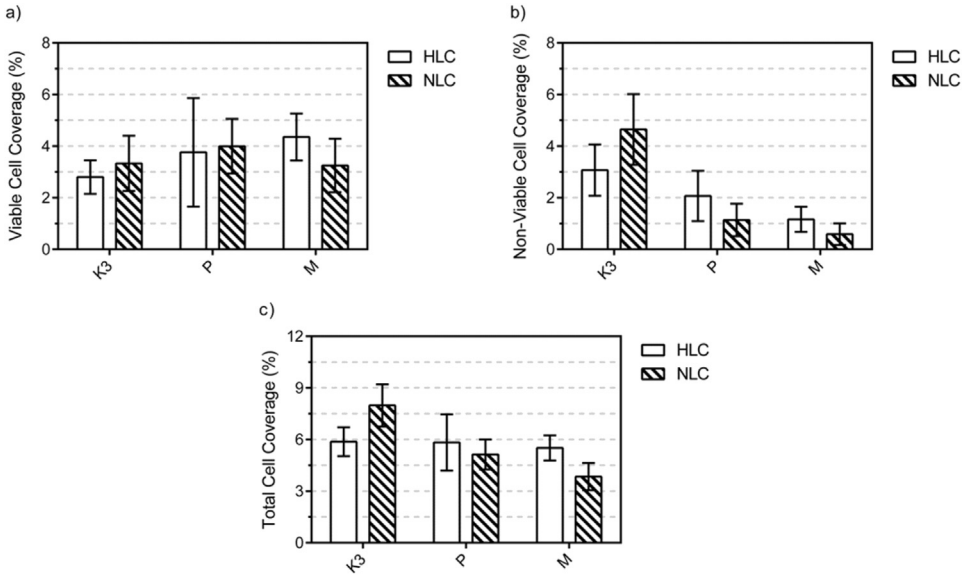

Fig. 3. Percent cell coverage of biofilm area at HLC and NLC (CLSM images acquired after three weeks of steady state operation); a) viable cell coverage, b) non-viable cell coverage, c) total (viable and non-viable) cell coverage.

substrates during the excessive overgrowth observed in the clogged M carriers (Tijhuis et al., 1994; Li et al., 2015). Hence, growth of newly formed biofilm may have been initiated after sloughing at NLC until the system reached steady state conditions. Therefore, at NLC it is likely that the upper biofilm of the M carries was newly generated biofilm (younger biofilm) that subsequently contained less non-viable cells compared to K3 carries that did not go through a sloughing event and maintained a mature upper biofilm with an

overall higher coverage of non-viable cells.

Although the biofilm thickness measurements of the P carrier do not demonstrate a large change in biofilm thickness between HLC and NLC, the P carriers are believed to have experienced excessive biofilm growth at the end of the HLC experimental phase. This excessive growth was not captured by the VPSEM imaging of the study and thus does not appear in Fig. 3. The excessive growth period, which occurred just prior to the transition to NLC, is believed to have caused a similar sloughing condition to the clogged M carriers and may be responsible for the observed lower coverage of non-viable cells as compared to the K3 carriers. The clogging at HLC observed in this study occurred in the carriers with the smallest pore spaces, where the M carrier (1200 m^2/m^3) clogged immediately, the P carrier (900 m^2/m^3) clogged at the end of the HLC and the K3 carrier (500 m^2/m^3) did not experience any clogging events in this study.

3.5. Bacterial population

Fig. S3 shows the phylogenetic tree identifying the core microbial phyla present within the biofilm samples analyzed in this study with the relative abundance of the genus of the various carriers at HLC and NLC. A dominance of *Proteobacteria* is observed in the samples, which is expected as synthetic wastewater with a low organic load was fed to all the reactors. Low organic loadings at both HLC and NLC were used to simulate nitrification conditions following conventional secondary treatment.

The OTUs were analyzed for overall variation using the uni-frac beta diversity in QIIME (Fig. 4). As mentioned above, 5 replications were run per sample and runs producing less than 15,000 reads were removed from the data set. The uni-frac beta diversity is a principal component analysis which identifies the OTUs most responsible for differentiation in the communities. This analysis is performed unweighted, presence/absence of OTUs, and weighted which takes the OTU relative abundance into account. The unweighted uni-frac beta diversity did not show significant separation with respect to HLC and NLC or carrier type. However, the weighted uni-frac beta diversity with respect to HLC and NLC does demonstrate clear separation in communities (Fig. 4a). Using an analysis of variance for distance matrices, it is found that there is a significant shift in populations comparing HLC and NLC conditions (ADONIS $R^2 = 0.13$, $p = 0.006$). Although this analysis does not identify the OTUs responsible for community separation, it does indicate the microbial ecology is affected by loading conditions. However Fig. 4b shows no clear separation between carrier types at equivalent loading conditions; indicating loading condition is the largest driver of microbial community population shifts. Additionally, the primary cause of separation between HLC and NLC in Fig. 4b is likely due to the observed shift in abundance of the species within the communities at the two operating conditions.

At both HLC and NLC, the family *Nitrosomonadacea* showed the highest relative abundance of ammonia oxidizing bacteria (AOB). Within the family *Nitrosomonadacea*, the genera *Nitrosomonas* and *Nitrosospira* were shown to be responsible for ammonia oxidation in this study. The genus *Nitrosococcus* was not detected in the samples even with *Nitrosococcus* being a suspected wastewater AOB in nitrifying systems (Daims and Nielsen, 2001; Gieseke et al., 2001; Park et al., 2008). At HLC and NLC, the family *Nitrospiraceae* showed the highest relative abundance of nitrite oxidizing bacteria (NOB). Within the family *Nitrospiraceae*, the genus *Nitrospira* was shown to be responsible for nitrite oxidation in this study. The genus *Nitrobacter*, a suspected wastewater NOB, was not detected in the samples.

Grouping the known AOB taxa shows that there is a significant decrease in AOB relative abundance from HLC to NLC (Fig. 5a). The average AOB relative abundance at HLC and NLC is 4.1 ± 0.9% and 7.2 ± 1.6% respectively, a ratio of 1:1.7. Although this appears counter intuitive, the biofilm thickness ratio at HLC to NLC is 2.6:1. As the NLC and HLC both demonstrate greater than 96% ammonia removal, HLC likely creates an environment suitable for other species of bacteria to be enriched in the biofilm matrix. This enrichment could partly cause the reduction in percent AOB cells

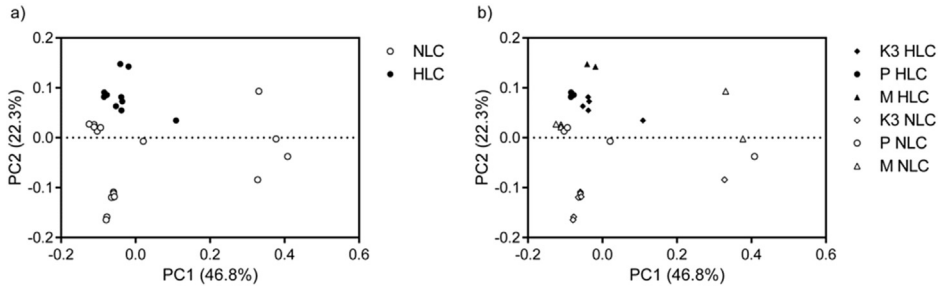

Fig. 4. Weighted uni-frac beta diversity measured after three weeks of steady state operation for a) HLC and NLC grouped, b) all sample groups.

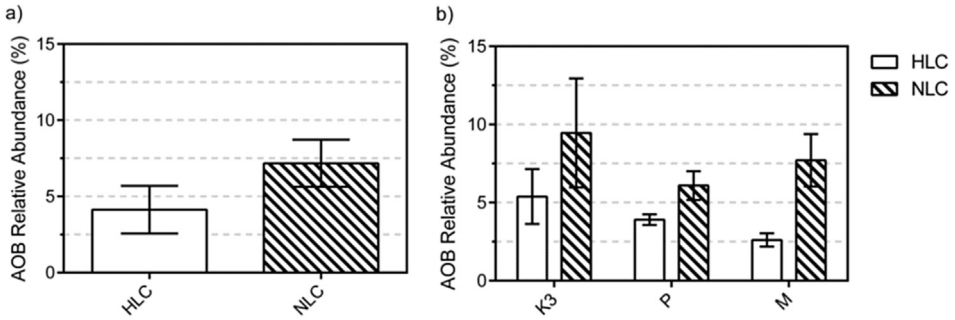

Fig. 5. Relative abundance measured after three weeks of steady state operation of a) AOB at HLC and NLC for all carriers and b) AOB embedded in the biofilm of each carrier type at HLC and NLC.

and the significant increase in biofilm thickness. The NOB remained constant at both HLC and NLC with relative abundances of 21.1 ± 7.0% and 23.9 ± 4.6% respectively.

The AOB relative abundance was also analyzed to determine the effects of carrier type on the population of AOB (Fig. 5b). The various carriers investigated in this study demonstrated similar relative abundance of AOB between the K3 carrier and the P carrier at HLC (Fig. 5b). The M carrier, being clogged at HLC, did demonstrate a significantly lower relative abundance of AOB as compared to the K3 and P carriers at HLC. The carriers demonstrated similar relative abundance of AOB across all studied carrier types at NLC. The NOBs in this study also were shown to not significantly change across carrier types.

To determine the differentially abundant species at HLC, the OTU table was analysed with metagenomeSEQ. This analysis allows for the determination of differentially abundant taxa with loading conditions as the main variable and carrier type as a covariate. For this analysis a positive $\log_2$ fold change indicates 76 unique taxa, which were abundant at statically different percent abundances at HLC as compared to NLC. The taxa belonged to three phyla, *Bacteroidetes*, *Firmicutes* and *Proteobacteria*, which are common in wastewater treatment plants and are diverse in their metabolic functionality.

At NLC the harvested samples are shown to be enriched with *Firmicutes*. Within this phylum, the most prominent differentially abundant genus is *Comamonas* with a $\log_2$ fold change of 24.04. *Comamonas* is a ubiquitous organism that is common in wastewater treatment plants and was likely outcompeted by the enriched bacteria in the HLC.

At HLC the samples are shown to be enriched with *Bacteroidetes* and *Proteobacteria*. Within these two phyla, the most prominent differentially abundant genera are *Zoogloea* and *Haliscomenobacter* with $\log_2$ fold changes of 4.86 and 7.28 respectively. *Zoogloea* and *Haliscomenobacter* are well known filamentous bulking organisms in conventional activated sludge treatment facilities (Aonofriesei and Petrosanu, 2007; Xue et al., 2012). Enrichment in filamentous bacteria, as low as 1% relative abundance, has been shown to lead to a decrease in sludge settlement (Kaewpipat and Grady, 2002; Martins et al., 2004). At HLC, *Zoogloea* and *Haliscomenobacter* represented 2.2% and 4.3% relative abundance as compared to 0.08% and 0.03% at NLC, respectively. This increase in filamentous bacteria is likely the cause of the poor settlement observed at HLC.

The microbial communities were also compared with respect to carrier type. As expected, the effect of differing carrier type produced fewer differentially abundant taxa than the effect of high versus conventional loading. The K3 carrier incorporated 8 differentially abundant taxa belonging to the *Proteobacteria* phylum as compared to the P and M carriers. The P carrier incorporated 6 differentially abundant taxa belonging to the *Planctomycetes* and *Proteobacteria* and phyla. Lastly, the M carrier incorporated 5 differentially abundant taxa belonging to the *Bacteroidetes*, *Firmicutes* and *Proteobacteria* phyla. All of the taxa identified were ubiquitous organisms and represented less than 0.2% relative abundance in the population. Thus the identification of the population shifts is an increase/reduction of few bacteria in the biofilm matrix.

3.6. Evaluation of cellular activity and bacterial population

The kinetics were normalized based on the biofilm morphology, cell viability and AOB relative abundance. At HLC the BVRR of the K3 and P carriers do not differ significantly, while the M carrier BVRR is significantly lower than both the K3 and P carriers (Table 1); indicating that the thicker biofilm on the M carrier at HLC is less efficient with respect to ammonia removal kinetics relative to total attached biofilm. At NLC there are significant differences between the BVRR values of the K3 carriers as compared to both the P and M carriers. Statistical difference are also observed between the BVRR values of the P and M carriers where the carrier with the highest surface area per volume, M, demonstrates the lowest BVRR (Table 1).

At HLC the VCRR of the K3 carriers are significantly higher than both the P and M carriers. The VCRR of the P carrier is significantly greater than the M carrier. Hence, the cells embedded in the K3 carriers, the carriers with the lowest surface area per volume, demonstrate a higher cellular activity than the carriers with the highest surface area per volume. At NLC, however, there were no statistical differences observed between the VCRR values of the carriers. The significant change in VCRR and BVRR of the M carrier could be influenced by the bulk liquid flow to the biofilm attached to the carriers and the subsequent mass transport through the biofilm. Although not studied for the specific carriers used in this study, the flow and mass transport through carrier pore spaces has been shown to be influenced by biofilm thickness and the filling of the pore spaces by biofilm (Herrling et al., 2014). The biofilm thickness of the M carrier in this study reduced the pore spaces of the M carrier, thus potentially decreasing the efficiency of flow through the carrier pore space and reducing the transport kinetics from the bulk liquid phase into the biofilm.

At HLC and NLC, no significant VAOBRR differences were observed across all carrier types investigated in this study (Table 1). This finding indicates that the viable AOBs present in the biofilm likely have similar kinetics irrespective of biofilm morphology, thickness or carrier type and irrespective of clogging conditions. Hence, these findings indicate that the clogged carriers do not decrease the AOB kinetics within the biofilm; instead clogging reduces the mass transfer rate likely through a reduction of the effective surface area of the attached biofilm. Further, this research shows that the viable AOBs present in the biofilm at HLC have faster kinetics as compared to the viable AOBs present at NLC, which is expected as larger quantities of ammonia are expected to be transferred to respective depths in the attached biofilm at higher loading conditions.

4. Conclusion

Post carbon removal nitrifying MBBR biofilm was studied over a period of 9 months at the meso and micro-scale with respect to

Table 1
Average and 95% confidence interval values of the biofilm volume ammonia removal rate (BVRR), the viable cell ammonia removal rate (VCRR) and the viable AOB ammonia removal rate (VAOBRR) at HLC and NLC measured across steady state.

Condition	Carrier type	BVRR × 10^3 (g-N/m^3 d)	VCRR × 10^3 (g-N/m^3 d·%viable cells)	VAOBRR (g-N/m^3 d·%viable AOB cells)
HLC	K3	10.6 ± 2.1	17.2 ± 2.0	264 ± 41
	P	8.54 ± 2.6	10.9 ± 1.8	281 ± 55
	M	1.9 ± 0.5	7.6 ± 1.6	280 ± 59
NLC	K3	19.6 ± 2.2	7.5 ± 1.7	81 ± 25
	P	5.8 ± 0.5	3.9 ± 0.7	85 ± 26
	M	2.8 ± 0.1	4.8 ± 0.4	63 ± 18

three different carrier types and two ammonia loading rates. The study shows the highest surface area to volume carriers demonstrate the highest propensity for clogging. The clogged pore spaces resulted in significantly lower ammonia removal rates and also the poorest solids settlement at HLC when compared to the other carriers. The research also shows that filamentous species were abundant under high loading conditions across all carriers, which likely resulted in the observed reduction in effluent solids settleability at high loading conditions as opposed to conventional loading conditions. The relative percentage of both live and dead cells at high and conventional loading were observed to remain stable for all carriers; where *Nitrosomonas* was found to be the dominant AOB and *Nitrospira* was the dominant NOB. The viable AOBs present in the biofilm at high loading appear to have faster kinetics as compared to the viable AOBs present at conventional loading. Moreover, the results suggest that clogging events reduce the effective surface area of the carriers but it does not appear to inhibit the cellular activity of the AOBs present in the biofilm. Finally, the study showed similar cellular activity rates of the AOB population irrespective of carrier type at both high and conventional loading conditions. Therefore, the research suggests that reactor performance cannot be predicted solely by the biofilm thickness, the biofilm mass per reactor, the bacterial percent abundance of ammonia oxidizing bacteria and the percentage of viable cells; instead post carbon removal MBBR ammonia removal kinetics is related to the viable AOB cell coverage of the carriers, which was calculated by normalizing the surface area removal rate by the biofilm thickness, the bacterial percent abundance of ammonia oxidizing bacteria and the percentage of viable cells.

Acknowledgments

The authors are grateful for the financial support from the Natural Science and Engineering Research Council of Canada (CRDPJ/436450-2012). The authors thank Edith Laflamme of Veolia Water Technologies Canada for her technical support.

Appendix A. Supplementary data

Supplementary data related to this article can be found at http://dx.doi.org/10.1016/j.watres.2016.01.006.

References

Abujamel, T., Cadnum, J.L., Sunkesula, V.C., Kundrapu, S., Jump, R.L., Stintzi, A.C., Donskey, C.J., 2013. Defining the vulnerable period for re-establishment of Clostridium difficile colonization after treatment of C. difficile infection with oral vancomycin or metronidazole. PLoS One 8 (10), e76269.

Aonofriesei, F., Petrosanu, M., 2007. Activated sludge bulking episodes and dominant filamentous bacteria at wastewater treatment plant constanta sud (Romania). Proc. Rom. Acad. 2, 83–87.

APHA, AWWA, WEF, 1998. Standard Methods for the Examination of Water and Wastewater. Washington, D.C.

Canada Gazette, 2012. Wastewater Systems Effluent Regulations, Part II. Government of Canada, Ottawa.

Caporaso, G.J., Lauber, C.L., Walters, W.A., Berg-Lyons, D., Lozupone, C.A., Turnbaugh, P.J., Fierer, N., Knight, R., 2010. Global patterns of 16S rRNA diversity at a depth of millions of sequences per sample. Proc. Natl. Acad. Sci. U. S. A. 4516–4522.

Daims, H., Nielsen, J.L., 2001. In situ characterization of Nitropira- like nitrite-oxidizing bacteria active in wastewater treatment plants. Am. Soc. Microbiol. 67 (11), 5273–5284.

Delatolla, R., Tufenkji, R., Comeau, Y., Gadbois, A., Lamarre, D., Berk, D., 2009a. Kinetic analysis of attached growth nitrification in cold climates. Water Sci. Technol. 60 (5), 1173–1184.

Delatolla, R., Tufenkji, R., Comeau, Y., Gadbois, A., Lamarre, D., Berk, D., 2009b. In situ characterization of nitrifying biofilm: minimizing biomass loss and preserving perspective. Water Res. 43, 1775–1787.

Flemming, H.-C., Szewzyk, U., Griebe, T., 2000. Biolms Investigative Methods & Applications. Technnomic, Pennsylvania.

Gerardi, M.H., 2002. Nitrogen: environmental and wastewater concerns. In: Nitrification and Denitrification in the Activated Sludge Process. John Wiley & Sons Inc, New York, pp. 3–9.

Gieseke, A., Purkhold, U., Wagner, M., Amamm, R., Schramm, A., 2001. Community structure and activity dynamics of nitrifying bacteria in a phosphate-removing biofilm. Clin. Microb. Rev. 67 (3), 1351–1362.

Gilbert, E.M., Agrawal, S., Schwartz, T., Horn, H., Lackner, S., 2015. Comparing different reactor configurations for partial Nitritation/Anammox at low temperatures. Water Res. 81, 92–100.

Goecks, J., Nekrutenko, A., Taylor, J., Team, T.G., 2010. Galaxy: a comprehensive approach for supporting accessible, reproducible, and transparent computational research in the life sciences. Genome Biol. 11, R86.

Herrling, M.P., Guthausen, G., Wagner, M., Lackner, S., Horn, H., 2014. Determining the flow regime in a biofilm carrier by means of magnetic resonance imaging. Biotechnol. Bioeng. 122 (5), 1023–1032.

Hoang, V., Delatolla, R., Abujamel, T., Mottawea, W., Gadbois, A., Laflamme, E., Stintzi, A., 2014. Nitrifying moving bed biofilm reactor (MBBR) biofilm and biomass response to long term exposure to 1 °C. Water Res. 49, 215–224.

Ivanovic, I., Leiknes, T.O., 2012. Particle separation in moving bed biofilm reactor: applications and opportunities. Sep. Sci. Technol. 47 (5), 647–653.

Ivanovic, I., Leiknes, T., Ødegaard, H., 2006. Influence of loading rates on production and characteristics of retentate from a biofil membrane bioreactor (BF-MBR). Desalination 199 (1–3), 490–492.

Kaewpipat, K., Grady Jr., C., 2002. Population dynamics in laboratory-scale activated sludge reactors. Water Sci. Technol. 46 (1–2), 19–27.

Karizmeh, M., Delatolla, R., Narbaitz, R., 2014. Investigation of settleability of biologically-produced solids and biofilm morphology in moving bed biofilm reactors (MBBRs). Bioprocess Biosyst. Eng. 37, 1158.

Lee, L.Y., Ong, S.L., Ng, W.J., 2004. Biofilm morphology and nitrification activities: recovery of nitrifying biofilm particles covered with heterotrophic outgrowth. Bioresour. Technol. 95 (2), 209–214.

Leyva-Díaz, J.C., Martín-Pascual, J., González-López, J., Hontoria, E., Poyatos, J.M., 2013. Effects of scale-up on a hybrid moving bed biofilm reactor – membrane bioreactor for treating urban wastewater. Chem. Eng. Sci. 104, 808–816.

Li, C., Wagner, M., Lackner, S., Horn, H., 2015. Assessing the influence of biofilm surface roughness on mass transfer by combining optical coherence tomography and two-dimensional modeling. Biotechnol. Bioeng. http://dx.doi.org/10.1002/bit.25868.

Majoc, T., Salzberg, S.L., 2011. FLASH: fast length adjustment of short reads to improve genome assemblies. Bioinformatics 27 (21), 2957–2963.

Martins, A., Pagilla, K., Heijnen, Loosdrecht, M., 2004. Filamentous bulking sludge – a critical review. Water Res. 38, 793–817.

Martín-Pascual, J., López-López, C., Cerdá, A., González-López, J., Hontoria, E., Poyatos, J.M., 2012. Comparative kinetic study of carrier type in a moving bed system applied to organic matter removal in urban wastewater treatment. Water Air Soil Pollut. 223 (4), 1699–1712.

Nogueira, R., Melo, L.s.F., Purkhold, U., Wuertz, S., Wagner, M., 2002. Nitrifying and heterotrophic population dynamics in biofilm reactors: effects of hydraulic retention time and the presence of organic carbon. Water Res. 36 (2), 469–481.

Ødegaard, H., Gisvold, B., Strickland, J., 2000. The influence of carrier size and shape in the moving bed biofilm process. Water Sci. Technol. 41 (4–5), 383–391.

Ødegaard, H., Rusten, B., Westrum, T., 1994. A new moving bed biofilm reactor-applications and results. Water Sci. Technol. 29 (10–11), 157–165.

Park, I., Zhao, R., West, J.A., Yabuuchi, A., Huo, H., Ince, T.A., Lerou, P.H., Lensch, M.W., Daley, G.Q., 2008. Reprogramming of human somatic cells to pluripotency with defined factors. Nature 451 (7175), 141–146.

Paulson, J., Stine, O., Bravo, H., Pop, M., 2013. Differential abundance analysis for microbial marker-gene surveys. Nat. Methods 10 (12), 1200–1202.

Rusten, B., Hem, L.J., Ødegaard, H., 1994. Nitrification in a moving bed biofilm reactor. Water Res. 28 (6), 1425–1433.

Tijhuis, L., Van Loosdrecht, M.C.C., Heijnen, J.J., 1994. Formation and growth of heterotrophic aerobic biofilms on small suspended particles in airlift reactors. Biotechnol. Bioeng. 44 (5), 595–608.

Wang, R., Wen, X., Qian, Y., 2005. Effect of carrier concentration on the performance and microbial characteristics of a suspended carrier biofilm reactor. Process Biochem. 40 (9), 2992–3001.

Water Environment Federation, 2011. Biofilm Reactors WEF MoP35. McGraw-Hill Professional, New York.

Xue, X., Zhang, K., Cai, F., Dai, J., Wang, Y., Rahman, E., Fang, C., 2012. Altherery-throbacter xinjiangenesis sp. nov., isolated from desert sand, and emended description of the genus Althererythrobacter. Int. J. Syst. Evol. Microbiol. 62 (1), 28–32.

Zhang, S., Wang, Y., He, W., Wu, M., Xing, M., Yang, J., Gao, N., Yin, D., 2013. Responses of biofilm characteristics to variations in temperature and NH_4^+-N loading in a moving bed biofilm reactor treating micro-polluted raw water. Bioresour. Technol. 131 (March), 365–373.